

# Quantum-classical path integral evaluation of reaction rates with a near-equilibrium flux formulation

Amartya Bose<sup>1</sup>  | Nancy Makri<sup>1,2</sup> 

<sup>1</sup>Department of Chemistry, University of Illinois, Urbana, Illinois

<sup>2</sup>Department of Physics, University of Illinois, Urbana, Illinois

## Correspondence

Nancy Makri, Department of Chemistry, University of Illinois, Urbana, IL 61801.  
Email: nmakri@illinois.edu

## Present address

Amartya Bose, Department of Chemistry, Princeton University, Princeton, New Jersey, 08544

## Funding information

National Science Foundation, Grant/Award Numbers: CHE 1665281, CHE 1955302

## Abstract

Quantum-classical formulations of reactive flux correlation functions require the partial Weyl–Wigner transform of the thermalized flux operator, whose numerical evaluation is unstable because of phase cancellation. In a recent paper, we introduced a non-equilibrium formulation which eliminates the need for construction of this distribution and which gives the reaction rate along with the time evolution of the reactant population. In this work, we describe a near-equilibrium formulation of the reactive flux, which accounts for important thermal correlations between the quantum system and its environment while avoiding the numerical instabilities of the full Weyl–Wigner transform. By minimizing early-time transients, the near-equilibrium formulation leads to an earlier onset of the plateau regime, allowing determination of the reaction rate from short-time dynamics. In combination with the quantum-classical path integral methodology, the near-equilibrium formulation offers an accurate and efficient approach for determining reaction rate constants in condensed phase environments. The near-equilibrium formulation may also be combined with a variety of approximate quantum-classical propagation methods.

## KEYWORDS

near-equilibrium, path integral, quantum-classical, reactive flux, reaction rate

## 1 | INTRODUCTION

Chemical reactions occur on timescales that span many orders of magnitude. While classical transition state theory [1, 2] offers a simple estimate of reaction rates for processes described by a potential barrier, large deviations are not uncommon. These are primarily associated with tunneling and other ubiquitous quantum mechanical effects, such as zero-point energy (which effectively lowers potential barriers), although classical effects responsible for the Kramers turnover [3–5] can also lead to significant deviations. In the case of nonadiabatic reactions, additional considerations come into play [6, 7]. A large body of work has been devoted to reaction rate theory and to the development of methods for calculating rates, and several excellent reviews are available [8–10].

Direct simulation of reactive processes can be prohibitive, even with the use of inexpensive classical trajectories, when the transformation of reactants to products is slow. Reactive flux formulations [8, 9, 11–23] circumvent this difficulty by following the dynamics only up to the relatively short “plateau” time. This time is reached once intra-well processes have settled and the reactant population has entered its slow exponential decay.

A variety of approaches have been pursued for calculating quantum mechanical reaction rates. In the case of condensed phase reactive processes and with the exception of system-harmonic bath models [24] (for which numerically exact treatments have been available since the 1990s [25]), reaction rate calculations are based on a variety of approximations. Formulations based on Feynman's path integral formulation of quantum statistical mechanics [26], in particular the dynamics of the centroid [27, 28] or the beads [29–31] of the path integral necklace (in the quantum-classical isomorphism [32]), have found many applications to a variety of processes.

A distinct approach involves the use of mixed quantum-classical treatments. Such treatments are easily justified in many reaction occurring in biological processes, where the majority of degrees of freedom are described by classical force fields, but can also provide accurate results in many other situations. This is so because strictly quantum mechanical effects arising from phase interference are effectively washed out in condensed phase processes, such that zero-point energy is the main quantum effect that needs to be accounted for in the description of the solvent atoms. Provided that quantization of the solvent equilibrium phase space density [2] is possible, all important quantum mechanical effects can be captured through an accurate treatment of the system coordinate.

Traditionally, quantum-classical methods invoke various prescriptions for calculating the influence of the quantum system on the classical trajectory of the solvent degrees of freedom. Ehrenfest's mean field prescription [33] is largely inadequate and often leads to unphysical results [34]. Surface hopping [35, 36] algorithms have found wide application, but cannot naturally account for decoherence effects induced by the solvent [37]. Rigorous quantum-classical formulations have emerged only recently. Such an approach is offered by the quantum-classical Liouville equation [38, 39], in particular its momentum-jump formulation [40, 41], although the computational demands of the method increase exponentially with propagation time. The other rigorous quantum-classical formulation is the quantum-classical path integral [42–44] (QCPI), which circumvents the Ehrenfest dilemma by replacing delocalized wavefunctions by local quantum paths, thus allowing an unambiguous determination of the force on the classical particles which is free of assumptions. The QCPI methodology has been shown to converge with modest effort in situations characteristic of charge or proton transfer reactions. An alternative to quantum-classical methods is offered by the Meyer–Miller mapping Hamiltonian [45, 46] bypasses the quantum-classical dilemma by replacing the quantum states by continuous degrees of freedom, which can subsequently be treated (along with the coordinates of the nuclei) by classical trajectory [47, 48] or imaginary-time path integral [49, 50] methods.

In this paper, we focus on the evaluation of reaction rates through quantum-classical methods. An important obstacle in this direction is the need for constructing the partial Wigner transform of the thermalized flux operator, which is necessary for a classical trajectory treatment of the solvent degrees of freedom. Numerical evaluation of the Wigner distribution [2] in multidimensional space is impractical because of the oscillating phase in the Fourier integral, which leads to the so-called “sign problem.” Several schemes have been proposed for constructing the Wigner distribution. These include local [51] or variationally optimized [52] Gaussian wavepacket approaches, and the thermal Gaussian approximation [53, 54] (which employ frozen Gaussian dynamics [55] in imaginary time), along with extensions that capture quantum corrections [56]. We recently introduced [57, 58] a simple, trajectory-based approximate procedure that makes use of the classical adiabatic theorem to slowly convert the Wigner density of a harmonic reference system to that of the target Hamiltonian. We also described a path integral representation of the Wigner density which exploits the coherent state representation to circumvent the numerical issues associated with the oscillatory Fourier phase [59]. Other recent work [60] has used the quasi-adiabatic propagator path integral methodology [61] to obtain the Wigner distribution of the bath in case of a system interacting with a bath of independent harmonic oscillators. However, these methods are not directly applicable to the present situation, where the target is the *partial* Weyl–Wigner transform with the system remaining in coordinate space.

In recent work [62] we circumvented this difficulty by introducing a non-equilibrium flux formulation which employs a simple initial condition that is easy to construct. As an additional benefit, the non-equilibrium formulation automatically generates the reactant population through the plateau time, offering a unified approach to the dynamics of slow as well as fast reactive processes. In the present paper, we propose a near-equilibrium formulation of the reactive flux, which reaches the plateau time earlier compared to the non-equilibrium method. In situations where accurate propagation is costly or impractical, the present approach offers an accurate, yet practical way of calculating reaction rates. The near-equilibrium formulation is based on a modification of the Weyl–Wigner transform of the thermalized flux operator, which is amenable to a path integral treatment and which is ideally suited to the QCPI treatment of the dynamics.

In Section 2 we describe the near-equilibrium formulation and the imaginary-time path integral representation of the thermalized flux. The QCPI implementation of the near-equilibrium flux correlation function is described in Section 3. In Section 4 the method is illustrated with application to dissipative two-level systems in various regimes. Some concluding remarks are given in Section 5.

## 2 | NEAR-EQUILIBRIUM FLUX FORMULATION

We consider a quantum system described by a coordinate  $s$ , in contact with a large number of degrees of freedom with coordinates and momenta  $\mathbf{q}, \mathbf{p}$ , which comprise the system's environment (or “solvent”). The total Hamiltonian is given by

$$\hat{H} = H_0(\hat{s}, \hat{\mathbf{p}}_s) + H_{\text{env}}(\hat{s}, \hat{\mathbf{q}}, \hat{\mathbf{p}}) = \hat{H}_0 + T_{\text{env}}(\hat{\mathbf{p}}) + V_{\text{env}}(\hat{s}, \hat{\mathbf{q}}), \quad (2.1)$$

where  $\hat{T}_{\text{env}}$  is the solvent kinetic energy operator, and  $V_{\text{env}}$  is the potential function that describes the interaction among solvent degrees of freedom and between solvent and system.

Reactive flux formulations are based on a separation of time scales, that is, the assumption that all non-reactive processes in the reactant potential well occur on a time scale much shorter than the time scale for completion of the reaction. This is often the case, as typical potential

barriers separating reactants and products are considerably larger than the thermal energy. Miller has shown [16, 17] that the (forward) rate constant for reactive processes in bimolecular collisions in the gas phase is given by the expression

$$k_+ = \lim_{t \rightarrow \infty} \text{Re} C_{fs}(t), \quad (2.2)$$

where

$$C_{fs}(t) = Z_R^{-1} \text{Tr} \left( e^{-i\hat{H}t/\hbar} e^{-\beta\hat{H}} \hat{F} e^{i\hat{H}t/\hbar} \hat{h}_R \right), \quad (2.3)$$

is the “flux-side” correlation function. Here  $\beta = 1/k_B T$ ,  $Z_R$  is the reactant partition function,  $\hat{h}_R$  is an operator that projects on the coordinates of the reactants, and

$$\hat{F} = \frac{i}{\hbar} [\hat{H}, \hat{h}_R]. \quad (2.4)$$

$\hat{F}$  is the flux operator. Note that  $\hat{H}_{\text{env}}$  commutes with  $\hat{h}_R$ , thus the flux operator acts only on the space of the system. For reactive processes in the condensed phase, Equation (2.2) is modified to

$$k_+ = \text{Re} C_{fs}(t) \Big|_{t \simeq t_{\text{plateau}}}, \quad (2.5)$$

where  $t_{\text{plateau}}$  is the “plateau time,” which signifies the end of early-time transients and the beginning of exponential decay for the reactant population. Assuming a separation of time scales, the plateau time occurs relatively early in the reactant-to-product transformation, thus  $k_+ t_{\text{plateau}} \ll 1$ . On a time scale much longer than  $t_{\text{plateau}}$ , the correlation function decays exponentially.

A variety of approaches may be employed to evaluate Equation (2.5). The present paper focuses on the use of quantum-classical methods. In such treatments the initial condition must be specified in terms of coordinate space for the quantum system and phase space variables for the environment. Thus, one needs to obtain the partial Weyl–Wigner transform [2, 63] of the operator  $e^{-\beta\hat{H}}\hat{F}$  with respect to the degrees of freedom comprising the system's environment,

$$W(s_0^\pm, \mathbf{q}_0, \mathbf{p}_0) = (2\pi\hbar)^{-n} \int d\xi \left\langle s_0^+, \mathbf{q}_0 + \frac{1}{2}\xi \left| e^{-\beta\hat{H}} \hat{F} \right| s_0^-, \mathbf{q}_0 - \frac{1}{2}\xi \right\rangle e^{-i\mathbf{p}_0 \cdot \xi / \hbar}. \quad (2.6)$$

Evaluation of this integral by means of Monte Carlo methods [64] is problematic, because of the oscillatory character of the Fourier factor, which leads to a sign problem.

To proceed, we take advantage of the invariance of the rate (in the exponential decay regime) with respect to details of the initial preparation of the system and its environment. In a recent paper [62] we exploited this independence by replacing the full Boltzmann operator by that corresponding to the solvent Hamiltonian. This procedure allowed the use of QCPI with a simple factorized initial condition corresponding to the solvent equilibrated with respect to the reactants. While the non-equilibrium initial density causes some delay to the onset of the flux plateau, we found that the plateau regime still occurs early on and thus is easily accessible to efficient dynamical treatments. In addition to obtaining the rate constant, knowledge of the flux from the non-equilibrium initial density allows direct determination of the transient population dynamics, thus providing a complete picture of the reactive process. In the present paper we propose the use of a near-equilibrium density which, while relatively easy to construct, leads to less pronounced transients and thus to a faster onset of the plateau. We emphasize that as long as Onsager's hypothesis is valid, both formulations produce the exact rate in condensed phase reactive processes.

The basic idea is to replace the exact Weyl–Wigner transform, Equation (2.6), by its product approximation,

$$W_0(s_0^\pm, \mathbf{q}_0, \mathbf{p}_0) \simeq P_{\text{pos}}(s_0^\pm, \mathbf{q}_0) P_{\text{mom}}(\mathbf{p}_0). \quad (2.7)$$

The position component is designed to give the exact coordinate distributions of the Weyl–Wigner function, that is,

$$P_{\text{pos}}(s_0^\pm, \mathbf{q}_0) = \int d\mathbf{p}_0 W(s_0^\pm, \mathbf{q}_0, \mathbf{p}_0), \quad (2.8)$$

while the momentum factor may satisfy an analogous relation, either exactly or approximately,

$$P_{\text{mom}}(\mathbf{p}_0) \simeq \int d\mathbf{q}_0 W(s_0^\pm, \mathbf{q}_0, \mathbf{p}_0) \Big|_{s_0^+ \text{ or } s_0^-}. \quad (2.9)$$

Using Equation (2.9) we obtain

$$\begin{aligned} P_{\text{pos}}(s_0^\pm, \mathbf{q}_0) &= (2\pi\hbar)^{-n} \int d\xi \left\langle s_0^+, \mathbf{q}_0 + \frac{1}{2}\xi \left| e^{-\beta\hat{H}\hat{F}} \right| s_0^-, \mathbf{q}_0 - \frac{1}{2}\xi \right\rangle \int d\mathbf{p}_0 e^{-i\mathbf{p}_0 \cdot \xi / \hbar} \\ &= \langle s_0^+ \mathbf{q}_0 | e^{-\beta\hat{H}\hat{F}} | s_0^- \mathbf{q}_0 \rangle. \end{aligned} \quad (2.10)$$

The position factor may be obtained from an imaginary-time path integral calculation. To this end, we express Equation (2.10) in discretized path integral form [65]. Defining the imaginary-time step  $\Delta\beta = \beta/M$  and employing a Trotter factorization, the high-temperature Boltzmann operator is expressed as

$$e^{-\Delta\beta\hat{H}} \simeq e^{-\frac{1}{2}\Delta\beta\hat{H}_{\text{env}}} e^{-\Delta\beta\hat{H}_0} e^{-\frac{1}{2}\Delta\beta\hat{H}_{\text{env}}} \simeq e^{-\frac{1}{2}\Delta\beta\hat{V}_{\text{env}}} e^{-\Delta\beta\hat{T}_{\text{env}}} e^{-\Delta\beta\hat{H}_0} e^{-\frac{1}{2}\Delta\beta\hat{V}_{\text{env}}}. \quad (2.11)$$

Thus the density matrix element in Equation (2.10) becomes

$$\begin{aligned} &\langle s_0^+ \mathbf{q}_0 | e^{-\beta\hat{H}\hat{F}} | s_0^- \mathbf{q}_0 \rangle \\ &= \langle s_0^+ \mathbf{q}_0 | e^{-\frac{1}{2}\Delta\beta\hat{V}_{\text{env}}} e^{-\Delta\beta\hat{T}_{\text{env}}} e^{-\Delta\beta\hat{H}_0} e^{-\Delta\beta\hat{V}_{\text{env}}} e^{-\Delta\beta\hat{T}_{\text{env}}} e^{-\Delta\beta\hat{H}_0} e^{-\Delta\beta\hat{V}_{\text{env}}} \dots e^{-\Delta\beta\hat{T}_{\text{env}}} e^{-\Delta\beta\hat{H}_0} e^{-\frac{1}{2}\Delta\beta\hat{V}_{\text{env}}} \hat{F} | s_0^- \mathbf{q}_0 \rangle. \end{aligned} \quad (2.12)$$

Following the standard procedure, we obtain the discretized path integral representation of (Equation 2.6),

$$\begin{aligned} \langle s_0^+ \mathbf{q}_0 | e^{-\beta\hat{H}\hat{F}} | s_0^- \mathbf{q}_0 \rangle &= \int ds_1 \dots \int ds_{M-1} \int d\mathbf{q}_1 \dots \int d\mathbf{q}_{M-1} e^{-\frac{1}{2}\Delta\beta V_{\text{env}}(s_0^+, \mathbf{q}_0)} \langle s_0^+ | e^{-\Delta\beta\hat{H}_0} | s_1 \rangle \langle \mathbf{q}_0 | e^{-\Delta\beta\hat{T}_{\text{env}}} | \mathbf{q}_1 \rangle \\ &\quad \times e^{-\Delta\beta V_{\text{env}}(s_1, \mathbf{q}_1)} \langle s_1 | e^{-\Delta\beta\hat{H}_0} | s_2 \rangle \langle \mathbf{q}_1 | e^{-\Delta\beta\hat{T}_{\text{env}}} | \mathbf{q}_2 \rangle e^{-\Delta\beta V_{\text{env}}(s_2, \mathbf{q}_2)} \dots \\ &\quad \times e^{-\Delta\beta V_{\text{env}}(s_{M-1}, \mathbf{q}_{M-1})} \langle s_{M-1} | e^{-\Delta\beta\hat{H}_0} \hat{F} | s_0^- \rangle \langle \mathbf{q}_{M-1} | e^{-\Delta\beta\hat{T}_{\text{env}}} | \mathbf{q}_0 \rangle e^{-\frac{1}{2}\Delta\beta V_{\text{env}}(s_0^-, \mathbf{q}_0)}. \end{aligned} \quad (2.13)$$

The variables in the space of the solvent degrees of freedom form the beads of a closed imaginary-time path integral necklace. Each of these beads interacts with the bead representing a path integral variable of the system coordinate. Since the system endpoints  $s_0^+, s_0^-$  are not necessarily identical, the necklace is open in the space of the system. A graphical illustration of the path integral necklace is given in Figure 1 for a case of a two-state system representing two diabatic potential surfaces.

In the general situation of a solvent described by anharmonic potentials functions, the integrals with respect to all path integral variables are to be performed by Monte Carlo. Note that if the solvent is described by a classical force field, which implicitly accounts for zero-point energy effects, one should not quantize the Boltzmann operator. The path integral expression of Equation (2.13) allows the use of different time slicing for system and solvent degrees of freedom. The details are given in Section 2.1, following the discussion of the momentum component.

The exact momentum factor, that is, the integral of the Weyl–Wigner transform with respect to solvent coordinates, is harder to obtain because of the oscillatory Fourier factor. However, knowledge of the precise form of the momentum component is not important for the purpose of determining the plateau value of the reactive flux. A variety of procedures may be used, depending on the nature of the solvent interactions. Below we describe procedures for the most common situations, along with the relevant adaptations of the coordinate factor, Equation (2.13):

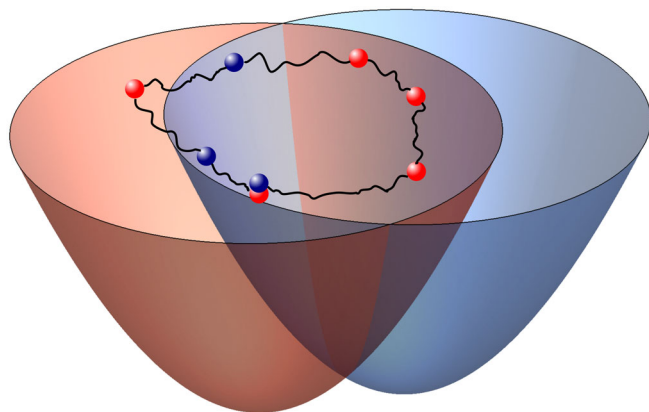


**FIGURE 1** Schematic illustration of the imaginary-time path integral necklace, Equation (2.13), for the case of a two-state system. The diabatic potential energy surfaces representing the reactant and product states (see also Section 4) are shown as red and blue surfaces in terms of two solvent coordinates  $q_1, q_2$ . The beads are colored red and blue to indicate the value of the system variable, which determines whether a bead is on the reactant or product surface

## 2.1 | Classical environment

If the solvent is described by classical force field, which captures some quantum mechanical effects, its Boltzmann factor should not be quantized. In this case the path integral necklaces for the solvent degrees of freedom collapse to a point and Equation (2.13) should be replaced by

$$\begin{aligned} \langle s_0^+ \mathbf{q}_0 | e^{-\beta \hat{H}} \hat{F} | s_0^- \mathbf{q}_0 \rangle &= \int ds_1 \dots \int ds_{M-1} e^{-\frac{1}{2} \Delta \beta V_{\text{env}}(s_0^+, \mathbf{q}_0)} \langle s_0^+ | e^{-\Delta \beta \hat{H}_0} | s_1 \rangle e^{-\Delta \beta V_{\text{env}}(s_1, \mathbf{q}_0)} \\ &\times \langle s_1 | e^{-\Delta \beta \hat{H}_0} | s_2 \rangle \dots \langle s_{M-1} | e^{-\Delta \beta \hat{H}_0} \hat{F} | s_0^- \rangle e^{-\frac{1}{2} \Delta \beta V_{\text{env}}(s_0^-, \mathbf{q}_0)}. \end{aligned} \quad (2.14)$$

Since no integrals with respect to solvent coordinates are required, Equation (2.14) may be evaluated by sequential matrix multiplications [66]. This procedure is simple and very efficient. In this case the momentum factor is given by the classical form,

$$P_{\text{mom}}(\mathbf{p}) = \exp\left(-\sum_{j=1}^n \frac{\beta}{2m_j} p_j^2\right). \quad (2.15)$$

## 2.2 | Harmonic environment

If the Hamiltonian of the environment is quadratic, for example, if it describes a harmonic bath or a situation where a normal mode analysis is meaningful, we use the harmonic Wigner momentum distribution

$$P_{\text{mom}}(\mathbf{p}) = \frac{1}{\sqrt{\pi}} \left(m\omega_j \hbar \coth \frac{1}{2} \hbar \omega_j \beta\right)^{\frac{1}{2}} \exp\left(-\sum_j \frac{\tanh \frac{1}{2} \hbar \omega_j \beta}{m\omega_j \hbar} p_j^2\right). \quad (2.16)$$

Evaluation of the position distribution may be done as in the general case Section 2.3. Alternatively, noting that in this case the system path integral variables in Equation (2.13) enter in a Gaussian fashion, one may integrate out these variables analytically to obtain an influence functional [67] that depends on the system path coordinates and the terminal bath coordinates  $\mathbf{q}_0$ . The remaining system variables may be integrated via standard Monte Carlo methods, or (in the case of a two-state system with small values of  $M$ ) through full quadrature.

## 2.3 | Anharmonic quantum environment

In this general situation, where the degrees of freedom comprising the system's environment are described by complex, anharmonic potential functions, the position factor is given by Equation (2.13). All integrals can be routinely performed by standard path integral Monte Carlo [64] methods.

There are various ways of obtaining a suitable momentum distribution in this general case. Perhaps the simplest approach is to assume a Gaussian momentum distribution for each particle, obtaining the coefficients from the average kinetic energy of each degree of freedom. From the harmonic oscillator model, one finds

$$P_{\text{mom}}(\mathbf{p}) = \left(\frac{a}{\pi}\right)^{\frac{1}{2}} \exp\left(-\sum_{j=1}^n a_j p_j^2\right), a_j = \frac{1}{2 \langle p_j^2 \rangle}. \quad (2.17)$$

Many algorithms are available for estimating the average kinetic energy and can be used to construct the momentum distribution.

## 3 | QUANTUM-CLASSICAL PATH INTEGRAL EVALUATION OF THE NEAR-EQUILIBRIUM FLUX

We now describe the use of the QCPI methodology for calculating the near-equilibrium flux. The QCPI representation of Equation (2.3) is

$$C_{fs}(N\Delta t) = Z_R^{-1} \sum_{s_0^\pm = R, P} \int d\mathbf{q}_0 d\mathbf{p}_0 W(s_0^\pm, \mathbf{q}_0, \mathbf{p}_0) Q(\mathbf{q}_0, \mathbf{p}_0, s_0^\pm, s_N^\pm = R, N\Delta t), \quad (3.1)$$

where

$$Q(\mathbf{q}_0, \mathbf{p}_0, s_0^\pm, s_N^\pm, N\Delta t) = \int ds_1 \dots \int ds_{M-1} \langle s_N^+ | U_{\text{ref}}(N\Delta t; (N-1)\Delta t, \mathbf{q}_0, \mathbf{p}_0) | s_{N-1}^+ \rangle \dots \\ \times \langle s_1^+ | U_{\text{ref}}(\Delta t; 0, \mathbf{q}_0, \mathbf{p}_0) | s_0^+ \rangle \langle s_0^- | U_{\text{ref}}(0; \Delta t, \mathbf{q}_0, \mathbf{p}_0) | s_1^- \rangle \\ \times \langle s_{N-1}^- | U_{\text{ref}}((N-1)\Delta t; N\Delta t, \mathbf{q}_0, \mathbf{p}_0) | s_N^- \rangle e^{i\varphi(\mathbf{q}_0, \mathbf{p}_0, s_0^\pm, \dots, s_N^\pm)/\hbar}, \quad (3.2)$$

is the quantum influence function [42, 43]. Here  $\varphi$  is the QCPI phase, which is evaluated from the action difference between forward and backward system paths along the particular solvent trajectory  $\mathbf{q}(t)$ ,  $\mathbf{p}(t)$  that is obtained from the initial phase space coordinates  $\mathbf{q}_0$ ,  $\mathbf{p}_0$  on a sequence of reactant-product potentials specified by the given forward-backward system path  $s_0^\pm, \dots, s_N^\pm$ , and  $\hat{U}_{\text{ref}}$  is the system propagator along a reference trajectory of the solvent [68].

The QCPI formulation employs energy-filtered propagators on a discrete system coordinate grid [61]. This representation allows the quadrature evaluation of the path integral with respect to system path variables, which circumvents the sign problem. Evaluation of the solvent factors is possible through a discrete variable representation of the path integral [69], which has the form of Equation (3.2) with all system integrals replaced by discrete sums,

$$Q(\mathbf{q}_0, \mathbf{p}_0, s_0^\pm, s_N^\pm, N\Delta t) = \sum_{s_1^+} \dots \sum_{s_{N-1}^+} \langle s_N^+ | U_{\text{ref}}(N\Delta t; (N-1)\Delta t, \mathbf{q}_0, \mathbf{p}_0) | s_{N-1}^+ \rangle \dots \\ \times \langle s_1^+ | U_{\text{ref}}(\Delta t; 0, \mathbf{q}_0, \mathbf{p}_0) | s_0^+ \rangle \langle s_0^- | U_{\text{ref}}(0; \Delta t, \mathbf{q}_0, \mathbf{p}_0) | s_1^- \rangle \\ \times \langle s_{N-1}^- | U_{\text{ref}}((N-1)\Delta t; N\Delta t, \mathbf{q}_0, \mathbf{p}_0) | s_N^- \rangle e^{i\varphi(\mathbf{q}_0, \mathbf{p}_0, s_0^\pm, \dots, s_N^\pm)/\hbar}, \quad (3.3)$$

where  $|s_k\rangle$  are the potential-optimized DVR states [70] and  $s_k$  the corresponding eigenvalues.

Using the simpler form of the Wigner function and its imaginary-time path integral representation, Equation (3.2) becomes

$$C_{fs}(N\Delta t) = Z_R^{-1} \sum_{s_0^\pm = R, P} \int d\mathbf{q}_0 \int d\mathbf{p}_0 \sum_{s_1} \dots \sum_{s_{M-1}} P_{\text{mom}}(\mathbf{p}_0) \int d\mathbf{q}_1 \dots \int d\mathbf{q}_{M-1} e^{-\frac{1}{2}\Delta\beta V_{\text{env}}(s_0^+, \mathbf{q}_0)} \\ \times \langle s_0^+ | e^{-\Delta\beta \hat{H}_0} | s_1 \rangle \langle \mathbf{q}_0 | e^{-\Delta\beta \hat{T}_{\text{env}}} | \mathbf{q}_1 \rangle e^{-\Delta\beta V_{\text{env}}(s_1, \mathbf{q}_1)} \langle s_1^- | e^{-\Delta\beta \hat{H}_0} | s_2 \rangle \langle \mathbf{q}_1 | e^{-\Delta\beta \hat{T}_{\text{env}}} | \mathbf{q}_2 \rangle \\ \times e^{-\Delta\beta V_{\text{env}}(s_2, \mathbf{q}_2)} \dots \langle s_{M-1}^- | e^{-\Delta\beta \hat{H}_0} | s_0^- \rangle \langle \mathbf{q}_{M-1} | e^{-\Delta\beta \hat{T}_{\text{env}}} | \mathbf{q}_0 \rangle e^{-\frac{1}{2}\Delta\beta V_{\text{env}}(s_0^-, \mathbf{q}_0)} \\ \times Q(\mathbf{q}_0, \mathbf{p}_0, s_0^\pm, s_N^\pm = R; N\Delta t) \quad (3.4)$$

The imaginary-time system propagators are evaluated exactly from the eigenstates of the system Hamiltonian [61], and the high-temperature kinetic energy Boltzmann matrix elements are given by the standard expression

$$\langle \mathbf{q}_k | e^{-\Delta\beta \hat{T}_{\text{env}}} | \mathbf{q}_{k+1} \rangle = \prod_{j=1}^n \sqrt{\frac{m_j}{2\pi\hbar^2\Delta\beta}} e^{-\frac{m_j}{2\hbar^2\Delta\beta}(q_{k+1} - q_k)^2}. \quad (3.5)$$

The integrals with respect to all solvent variables, that is, the trajectory initial conditions  $\mathbf{q}_0$ ,  $\mathbf{p}_0$  and the imaginary time path integral variables  $\mathbf{q}_1, \dots, \mathbf{q}_M$ , as well as the sums with respect to the imaginary-time system variables  $s_1, \dots, s_{M-1}$  are performed by Monte Carlo. The un-normalized sampling function is the integrand of Equation (2.13) multiplied by the momentum factor  $P_{\text{mom}}(\mathbf{p}_0)$ . Normalization is achieved by dividing the Monte Carlo average by that obtained by replacing the quantum influence function by unity. Notice that the reactant partition function cancels out in this process and thus does not need to be evaluated.

The quantum influence function, Equation (3.2), is computed using the iterative QCPI methodology, which maintains a constant number of classical trajectories [43]. In the common case of an initial density matrix that is diagonal in the system basis, use of a dynamically consistent state hopping (DCSH) procedure [71] leads to accelerated convergence. However, in the present case where the system initial condition includes off-diagonal components implementation of the DCSH procedure is not straightforward, so we revert to the original, random choice of branching trajectories.

## 4 | NUMERICAL EXAMPLES

We illustrate the near-equilibrium flux formulation on a model system of two states, which represent the reactants “R” and products “P” of a charge transfer reaction or a double well potential at low temperatures. The system operator is expressed as

$$\hat{s} = |R\rangle\langle R| - |P\rangle\langle P|, \quad (4.1)$$

and the Hamiltonian describing the system has the general form

$$\hat{H}_0 = -\hbar\Omega(|R\rangle\langle P| + |P\rangle\langle R|) + \varepsilon(|R\rangle\langle R| - |P\rangle\langle P|). \quad (4.2)$$

In this case the projector on reactant space has the form  $\hat{h}_R = |R\rangle\langle R|$  is an operator that projects on reactants (labeled “R”), and the flux operator is

$$\hat{F} = i\Omega(|R\rangle\langle P| - |P\rangle\langle R|). \quad (4.3)$$

The Hamiltonian of the environment is described by a harmonic bath,

$$\hat{T}_{\text{env}} = \sum_j \frac{\hat{p}_j^2}{2m_j}, \quad \hat{V}_{\text{env}} = \frac{1}{2}m_j\omega_j^2\hat{q}_j^2 - c_j\hat{s}\hat{q}_j. \quad (4.4)$$

The frequencies and the couplings of the bath are collectively characterized by a spectral density function [72]. Here we use the Ohmic form with an exponential cutoff,

$$J(\omega) = \frac{1}{2}\pi\xi\hbar\omega e^{-\omega/\omega_c}, \quad (4.5)$$

where  $\xi$  is the Kondo parameter and  $\omega_c$  is the cutoff frequency.

We choose a symmetric system ( $\varepsilon = 0$ ) with the parameters used by Topaler and Makri [73], where the two-level system (TLS) coupling corresponds to a tunneling splitting  $2\hbar\Omega = 0.00105 \text{ cm}^{-1}$  and the cutoff frequency is  $\omega_c = 500 \text{ cm}^{-1}$ . These parameters are characteristic of many proton transfer reactions. The small tunneling splitting is a result of a high potential barrier, while the frequencies of the bath degrees of freedom are much higher, leading to a clean separation of time scales and a relatively short plateau time.

The classical trajectories employed in the QCPI methodology require discrete bath degrees of freedom. For this purpose the harmonic bath was discretized into 300 modes using the logarithmic discretization scheme [74, 75] with  $\omega_{\text{max}} = 4\omega_c$ . We used  $3 \times 10^3$  Monte Carlo points per bath mode to shrink the statistical error in the correlation function to values smaller than the marker size in the figures.

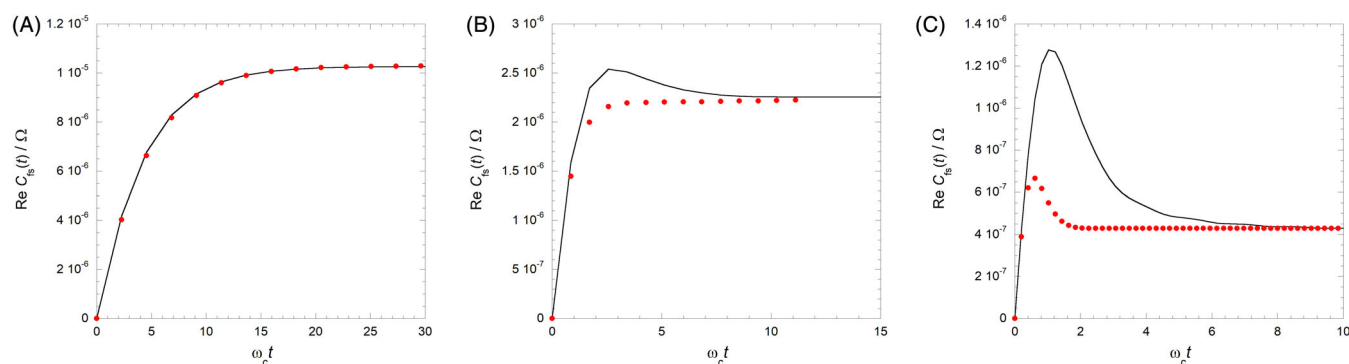


**FIGURE 2** Comparison of the non-equilibrium flux method [62] and the present near-equilibrium flux method at room temperature and three values of the system-bath coupling. Solid line: Non-equilibrium flux. Red markers: Near-equilibrium flux. Left (or top):  $\xi = 0.1$ . Middle:  $\xi = 0.5$ . Right (or bottom):  $\xi = 1.5$

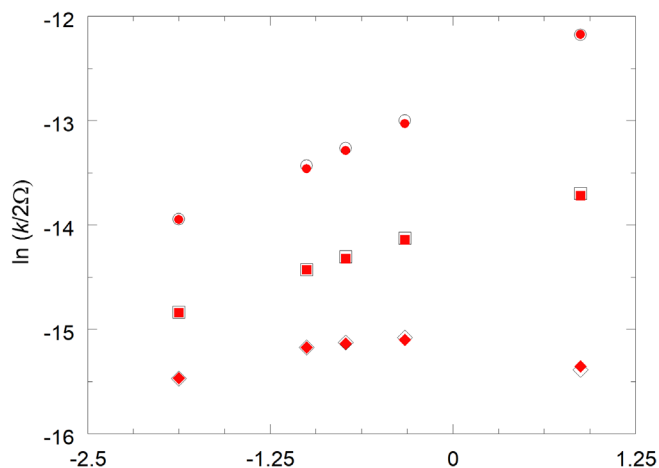


**FIGURE 3** Rates at different parameters. Black hollow shapes: Non-equilibrium flux method. Red filled shapes: Near-equilibrium initial condition. Circles:  $\xi = 0.1$ . Squares:  $\xi = 0.5$ . Diamonds:  $\xi = 1.5$

Figure 2 shows the time evolution of the reactive flux at  $T = 300$  K for three values of the system-bath coupling strength,  $\xi = 0.1, 0.5$ , and  $1.5$ . Results obtained with the current near-equilibrium flux approach, where the time evolution was obtained through the QCPI methodology, are compared to those obtained through the simpler non-equilibrium flux scheme [62] with the propagation of the initial density was obtained with the quasiadiabatic propagator path integral [76, 77] (QuAPI) algorithm. At small values of the system-bath coupling the two side-flux correlation functions do not exhibit notable differences. However, as the coupling is increased, transients in the dynamics become significant. As is seen from Figure 2, these transients are considerably less pronounced in the near-equilibrium flux, and this correlation function plateaus earlier in the cases where the bath is coupled strongly to the system. As expected, the long-time rates obtained by the two methods are identical. The earlier plateau attained by the near-equilibrium flux allows the rate to be obtained from shorter time propagation.

In Figure 3 we show the rate as a function of inverse temperature for the three values of system-bath coupling. The results obtained with the two methods are in quantitative agreement and practically identical to those obtained by Topaler and Makri.

## 5 | CONCLUDING REMARKS

We have described a near-equilibrium formulation of reactive flux correlation functions suitable for quantum-classical calculations. Rather than constructing the required partial Weyl–Wigner transform through numerically unstable multidimensional integration procedures, we use a factorized approximation to this distribution which is amenable to accurate evaluation by robust imaginary-time path integral methods. This distribution accounts for the entanglement of system and solvent and is much closer to the full Weyl–Wigner transform of the thermalized flux operator compared to the analogous distribution employed in the non-equilibrium rate formulation. As a result, initial transients die out more rapidly and the plateau regime is reached faster. This advantage was illustrated clearly through calculations of a model two-state system interacting with a dissipative bath over a range of temperatures and system-bath coupling strength.

Clearly, the gains achieved through the faster emergence of the plateau regime should be weighed against the additional complexity and cost associated with the imaginary-time path integral representation of the Boltzmann operator, as well as the determination of kinetic energy factors required to construct an accurate momentum factor in the most general situation. In many situations where iterative QCPI or QuAPI (and its powerful small-matrix path integral decomposition [78, 79]) algorithms are viable, the non-equilibrium formulation offers the preferred approach. However, in more demanding situations where long-time propagation is problematic, as in cases of very long solvent-induced memory, the present near-equilibrium formulation can enable the determination of the rate constant without the need for iterative propagation outside of the memory interval. Thus the present formulation can be valuable for characterizing reactive processes in condensed phase environments which are not amenable to other rigorous treatments.

Last, we note that the near-equilibrium flux formulation with the path integral procedure developed in Section 2 may be used in connection with less accurate quantum-classical propagation schemes. Since the accuracy of approximate methods typically degrades with propagation time, the faster establishment of the plateau regime through the near-equilibrium flux formulation would increase the accuracy of the obtained rate constant. Thus, the combination of the near-equilibrium flux formulation with commonly employed quantum-classical methods can lead to many applications in chemical and biological systems.

## ACKNOWLEDGMENTS

This material is based upon work supported by the National Science Foundation under Awards CHE-1665281 and 1955302.

## AUTHOR CONTRIBUTIONS

**Amartya Bose:** Conceptualization; data curation; formal analysis; methodology; writing-original draft; writing-review & editing.

## DATA AVAILABILITY STATEMENT

The data that support the findings of this study are available from the corresponding author upon reasonable request.

## ORCID

Amartya Bose  <https://orcid.org/0000-0003-0685-5096>

Nancy Makri  <https://orcid.org/0000-0002-3310-7328>

## REFERENCES

- [1] H. Eyring, *J. Chem. Phys.* **1935**, *3*, 107.
- [2] E. J. Wigner, *J. Chem. Phys.* **1937**, *5*, 720.
- [3] H. A. Kramers, *Physica (Utrecht)* **1940**, *7*, 284.
- [4] R. F. Grote, J. T. Hynes, *J. Chem. Phys.* **1980**, *73*, 2715.
- [5] E. Pollak, *J. Chem. Phys.* **1986**, *85*, 865.
- [6] R. A. Marcus, N. Sutin, *Biochim. Biophys. Acta* **1985**, *811*, 265.
- [7] H. Frauenfelder, P. G. Wolynes, *Science* **1985**, *228*, 337.
- [8] P. Hänggi, P. Talkner, M. Borcovec, *Rev. Mod. Phys.* **1990**, *62*, 251.
- [9] W. H. Miller, *Faraday Discuss.* **1998**, *110*, 1.
- [10] E. Pollak, P. Talkner, *Chaos* **2005**, *15*, 026116.
- [11] R. Kubo, *J. Phys. Soc. Jpn.* **1957**, *12*, 570.
- [12] T. Yamamoto, *J. Chem. Phys.* **1960**, *33*, 281.
- [13] J. C. Keck, *J. Chem. Phys.* **1960**, *32*, 1035.
- [14] J. C. Keck, *Adv. Chem. Phys.* **1967**, *13*, 85.
- [15] R. Kapral, *J. Chem. Phys.* **1972**, *56*, 1842.
- [16] W. H. Miller, *J. Chem. Phys.* **1974**, *61*, 1823.
- [17] W. H. Miller, S. D. Schwartz, J. W. Tromp, *J. Chem. Phys.* **1983**, *79*, 4889.
- [18] D. Chandler, *J. Chem. Phys.* **1978**, *68*, 2959.
- [19] D. Chandler, *Introduction to Modern Statistical Mechanics*, Oxford University Press, New York **1987**.
- [20] B. J. Berne, in *Multiple time scales* (Eds: J. U. Brackbill, B. I. Cohen), Academic Press, New York **1985**, p. 419.
- [21] B. J. Berne, in *Activated Barrier Crossing: Application in Physics, Chemistry and Biology* (Eds: G. R. Fleming, P. Hänggi), World Scientific Publishing Co. Pt. Ltd., Singapore **1993**, p. 82.
- [22] G. Ciccotti, in *Proceedings of the NATO ASI on Computer Simulation in Materials Science* (Eds: M. Meyer, V. Pontikis), Kluwer, Dordrecht **1991**, p. 119.
- [23] E. Pollak, J.-L. Liao, *J. Chem. Phys.* **1998**, *108*, 2733.
- [24] A. O. Caldeira, A. J. Leggett, *Ann. Phys.* **1983**, *149*(2), 374.
- [25] N. Makri, *J. Math. Phys.* **1995**, *36*, 2430.
- [26] R. P. Feynman, *Statistical Mechanics*, Addison-Wesley, Redwood City **1972**.
- [27] G. A. Voth, D. Chandler, W. H. Miller, *J. Chem. Phys.* **1989**, *91*, 7749.
- [28] G. A. Voth, *Advances in Chemical Physics*, *93*, **1996**, 135.
- [29] I. R. Craig, D. E. Manolopoulos, *J. Chem. Phys.* **2004**, *121*, 3368.
- [30] J. Richardson, S. Althorpe, *J. Chem. Phys.* **2009**, *131*, 214106.
- [31] S. Habershon, D. E. Manolopoulos, T. E. Markland, T. F. Miller III., *Annu. Rev. Phys. Chem.* **2013**, *64*, 387.
- [32] D. Chandler, P. G. Wolynes, *J. Chem. Phys.* **1981**, *74*, 4078.
- [33] P. Ehrenfest, *Z. Phys.* **1927**, *45*, 455.
- [34] J. C. Tully, *Faraday Disc.* **1998**, *110*, 407.
- [35] J. C. Tully, R. K. Preston, *J. Chem. Phys.* **1971**, *55*, 562.
- [36] J. C. Tully, *J. Chem. Phys.* **1990**, *93*, 1061.
- [37] J. E. Subotnik, A. Jain, B. Landry, A. Petit, W. Ouyang, N. Bellonzi, *Annu. Rev. Phys. Chem.* **2016**, *67*, 387.
- [38] A. Donoso, C. C. Martens, *J. Phys. Chem. A* **1998**, *102*, 4291.
- [39] R. Kapral, G. Ciccotti, *J. Chem. Phys.* **1999**, *110*, 8919.
- [40] D. Mac Kernan, G. Ciccotti, R. Kapral, *J. Phys.: Condens. Matter* **2002**, *14*, 9069.
- [41] D. Mac Kernan, G. Ciccotti, R. Kapral, *J. Phys. Chem. B* **2008**, *112*, 424.
- [42] R. Lambert, N. Makri, *J. Chem. Phys.* **2012**, *137*, 22A552.
- [43] R. Lambert, N. Makri, *J. Chem. Phys.* **2012**, *137*, 22A553.
- [44] N. Makri, *Int. J. Quantum Chem.* **2015**, *115*, 1209.
- [45] H.-D. Meyer, W. H. Miller, *J. Chem. Phys.* **1979**, *70*, 3214.
- [46] G. Stock, M. Thoss, *Phys. Rev. Lett.* **1997**, *78*, 578.
- [47] H. Wang, X. Sun, W. H. Miller, *J. Chem. Phys.* **1998**, *108*, 9726.
- [48] W. H. Miller, S. J. Cotton, *Faraday Disc.* **2017**, *195*, 9.
- [49] N. Ananth, T. F. Miller, *J. Chem. Phys.* **2010**, *133*, 234103.
- [50] N. Ananth, *J. Chem. Phys.* **2013**, *139*, 124102.

- [51] Q. Shi, E. Geva, *J. Phys. Chem. A* **2003**, *107*, 9059.
- [52] J. A. Poulsen, G. Nyman, P. J. Rossky, *J. Chem. Phys.* **2003**, *119*(23), 12179.
- [53] J. Liu, W. H. Miller, *J. Chem. Phys.* **2006**, *125*, 224104.
- [54] J. Liu, *Int. J. Quantum Chem.* **2015**, *115*, 657.
- [55] E. J. Heller, *J. Chem. Phys.* **1976**, *64*, 63.
- [56] J. Shao, E. Pollak, *J. Chem. Phys.* **2006**, *125*, 133502.
- [57] A. Bose, N. Makri, *J. Chem. Phys.* **2015**, *143*, 114114.
- [58] A. Bose, N. Makri, *J. Chem. Theory Comput.* **2018**, *14*, 5446.
- [59] A. Bose, N. Makri, *J. Phys. Chem. A* **2019**, *123*, 4284.
- [60] A. Montoya-Castillo, D. R. Reichman, *J. Chem. Phys.* **2017**, *146*, 084110.
- [61] N. Makri, *Chem. Phys. Lett.* **1992**, *193*, 435.
- [62] A. Bose, N. Makri, *J. Chem. Phys.* **2017**, *147*, 152723.
- [63] H. Weyl, *Z. Phys.* **1927**, *46*, 1.
- [64] N. Metropolis, A. W. Rosenbluth, M. N. Rosenbluth, H. Teller, E. Teller, *J. Chem. Phys.* **1953**, *21*, 1087.
- [65] R. P. Feynman, *Rev. Mod. Phys.* **1948**, *20*, 367.
- [66] D. Thirumalai, E. J. Bruskin, B. J. Berne, *J. Chem. Phys.* **1983**, *79*, 5063.
- [67] R. P. Feynman, J. F. L. Vernon, *Ann. Phys.* **1963**, *24*, 118.
- [68] T. Banerjee, N. Makri, *J. Phys. Chem.* **2013**, *117*, 13357.
- [69] M. Topaler, N. Makri, *Chem. Phys. Lett.* **1993**, *210*, 448.
- [70] J. Echave, D. C. Clary, *J. Chem. Phys.* **1992**, *190*, 225.
- [71] P. L. Walters, N. Makri, *J. Chem. Phys.* **2016**, *144*, 044108.
- [72] A. O. Caldeira, A. J. Leggett, *Phys. A* **1983**, *121*, 587.
- [73] M. Topaler, N. Makri, *J. Chem. Phys.* **1994**, *101*, 7500.
- [74] N. Makri, *J. Phys. Chem.* **1999**, *103*, 2823.
- [75] P. L. Walters, T. C. Allen, N. Makri, *J. Comput. Chem.* **2017**, *38*, 110.
- [76] N. Makri, D. E. Makarov, *J. Chem. Phys.* **1995**, *102*, 4600.
- [77] N. Makri, D. E. Makarov, *J. Chem. Phys.* **1995**, *102*, 4611.
- [78] N. Makri, *J. Chem. Phys.* **2020**, *152*, 041104.
- [79] N. Makri, *J. Chem. Theory Comput.* **2020**, *16*, 4038.

**How to cite this article:** Bose A, Makri N. Quantum-classical path integral evaluation of reaction rates with a near-equilibrium flux formulation. *Int J Quantum Chem.* 2021;121:qua26618. <https://doi.org/10.1002/qua.26618>